*EJPMR, 2025, 12(10), 445-456* **Research Article** **Impact Factor 7.065**

**EUROPEAN JOURNAL OF PHARMACEUTICAL AND MEDICAL RESEARCH**

www.ejpmr.com

**ISSN (O): 2394-3211**
**ISSN (P): 3051-2573**
**Coden USA: EJPMAG**

# DEVELOPMENT AND CHARACTERIZATION OF DIBUCAINE-LOADED SOLID LIPID NANOPARTICLES BY HIGH-PRESSURE HOMOGENIZATION FOR ENHANCED LOCAL ANESTHETIC EFFICACY AND SAFETY

**Pankaj Gill[1], Dr. Umesh Kumar*[2]**

[1,2]School of Pharmaceutical Sciences, Shri Venkateshwara University, Gajraula, UP, India.

***Corresponding Author: Prof. Dr. Umesh Kumar**

School of Pharmaceutical Sciences, Shri Venkateshwara University, Gajraula, UP, India.

**DOI:** https://doi.org/10.5281/zenodo.18465107

**How to cite this Article:** Pankaj Gill1, Dr. Umesh Kumar*2, (2025). Development And Characterization Of Dibucaine-Loaded Solid Lipid Nanoparticles By High-Pressure Homogenization For Enhanced Local Anesthetic Efficacy And Safety. European Journal of Pharmaceutical and Medical Research, 12(10), 445–456.


**Article Received on 21/08/2025** **Article Revised on 11/10/2025** **Article Published on 23/12/2025**

## ABSTRACT

Dibucaine (DBC), a highly potent amide-type local anesthetic, is limited in clinical use by poor aqueous solubility, rapid systemic absorption, and narrow therapeutic index, which increase risks of CNS and cardiovascular toxicity. This study aimed to develop and comprehensively characterize DBC-loaded solid lipid nanoparticles (SLNs) using high-pressure homogenization to achieve sustained release, enhanced local efficacy, and improved safety profile. SLNs were prepared with myristyl myristate (SLNM) or cetyl palmitate (SLNCP) as lipid matrices (5% w/v), stabilized by Pluronic F68 (1% w/v), and loaded with 0.5% w/v DBC. The formulations exhibited high encapsulation efficiency (92.4 ± 2.1% for SLNM; 89.7 ± 1.8% for SLNCP), nanoscale hydrodynamic diameters (148.7 ± 3.9 nm and 162.4 ± 4.1 nm, respectively), low polydispersity indices (<0.25), and strongly negative zeta potentials (–29.6 to –32.1 mV), remaining stable over 240 days at 4°C. Transmission electron microscopy confirmed spherical morphology with distinct core-shell architecture. Differential scanning calorimetry revealed reduced crystallinity (74–77%), while electron paramagnetic resonance demonstrated increased lipid fluidity upon DBC incorporation. In vitro release studies showed biphasic, sustained Fickian diffusion profiles (Weibull $\beta < 0.75$; Korsmeyer-Peppas $n < 0.44$), with 72.4% and 68.7% cumulative release at 48 h from SLNM and SLNCP, respectively, compared to rapid release of free DBC. MTT assays on BALB/c 3T3 fibroblasts and HaCaT keratinocytes indicated significantly reduced cytotoxicity (>85% viability at 2.1 mmol/L vs. <60% for free DBC). In vivo tail-flick tests in Wistar rats demonstrated prolonged antinociception, with recovery time extended by 142% (SLNM) and 128% (SLNCP) compared to free DBC ($p < 0.01$). These results establish DBC-loaded SLNs as a promising, biocompatible nanoplatform for safer, longer-acting local anesthesia, with potential applications in infiltrative and postoperative pain management.

**KEYWORDS:** Dibucaine, Solid Lipid Nanoparticles, High-Pressure Homogenization, Sustained Release, Local Anaesthesia.

## 1. INTRODUCTION

Local anaesthetics (LAs) play a critical role in pain management, particularly in surgical and dental procedures, labour analgesia, and postoperative care. Among these, Dibucaine (DBC), also known as cinchocaine, is an amide-type local anaesthetic that exhibits higher potency and prolonged duration of action compared to conventional anaesthetics like lidocaine and bupivacaine (Chowdhury et al., 2017). Despite its favourable pharmacodynamic properties, the clinical application of DBC remains limited due to its poor aqueous solubility and a narrow therapeutic index, which leads to significant systemic toxicity when administered in conventional forms (Patel et al., 2021).

The therapeutic efficacy of local anesthetics is often compromised by rapid drug clearance, short duration of action, and the need for frequent administration. These drawbacks contribute not only to reduced patient compliance but also to increased risk of systemic adverse effects, including central nervous system (CNS) toxicity and cardiotoxicity (Becker & Reed, 2012). In the case of

DBC, these issues are particularly severe due to its high lipophilicity and rapid systemic absorption from vascular tissues, often leading to peak plasma levels that can trigger seizures, bradycardia, or even cardiac arrest (Gupta et al., 2019).

To overcome these challenges, novel drug delivery systems are being explored. One such approach involves the use of Solid Lipid Nanoparticles (SLNs), a class of lipid-based nanocarriers that has gained prominence due to their biocompatibility, scalability, and ability to encapsulate lipophilic drugs like DBC (Müller et al., 2000). SLNs are submicron colloidal carriers composed of physiological lipids, typically in the size range of 50–1000 nm, and stabilized by surfactants in aqueous dispersion. These systems are known to improve drug solubility, provide controlled and sustained drug release, and reduce burst effects and systemic exposure (Doktorovová et al., 2014).

SLNs offer several advantages over conventional formulations and other nanosystems such as liposomes and polymeric nanoparticles. They demonstrate excellent physical stability, high drug-loading efficiency, and are produced using cost-effective techniques like high-pressure homogenization (Mehnert & Mäder, 2001). Their solid lipid matrix can protect the encapsulated drug from enzymatic degradation, especially in physiological fluids, and their ability to adhere to biological membranes enhances local bioavailability (Garud et al., 2012).

Previous research has shown that local anaesthetics encapsulated in lipid-based carriers can prolong anaesthesia duration and reduce toxicity. For instance, liposomal formulations of bupivacaine have been approved for postoperative pain control, offering extended analgesia up to 72 hours (Ilfeld & Viscusi, 2018). However, similar delivery platforms for DBC are lacking in the current pharmacopeia. Given its superior potency and duration, DBC is an ideal candidate for nanotechnology-based sustained-release formulations, which could address both solubility and safety concerns (Jain et al., 2022).

The present study aims to develop and characterise a DBC-loaded SLN formulation to improve its therapeutic index, reduce toxicity, and enhance its clinical applicability. By employing high-pressure homogenization, this work evaluates the physicochemical characteristics, in vitro drug release profile, and biocompatibility of the developed nanoparticles. The long-term goal is to establish SLNs as a robust platform for delivering DBC in a safer, more effective manner, particularly for infiltrative anaesthesia and postoperative pain management.

## 2. MATERIALS AND METHODOLOGY

### 2.1. Materials

Dibucaine (DBC), myristyl myristate (MM), cetyl palmitate (CP), and Pluronic F68 (poloxamer 188) were obtained from Sigma-Aldrich (St. Louis, MO, USA) with purities≥99%. Analytical-grade reagents, including acetonitrile, triethylamine, phosphoric acid, sodium chloride, and phosphate buffer salts, were sourced from Merck KGaA (Darmstadt, Germany). Milli-Q water (resistivity 18.2 MΩ·cm) was produced using a Milli-Q Direct 8 system (Merck Millipore, Billerica, MA, USA) and used for all aqueous preparations. Cell culture media, including Dulbecco's Modified Eagle Medium (DMEM) and fetal bovine serum (FBS), were purchased from Gibco (Thermo Fisher Scientific, Waltham, MA, USA). The 3-(4,5-dimethylthiazol-2-yl)-2,5-diphenyltetrazolium bromide (MTT) reagent was acquired from Sigma-Aldrich. All materials were stored under recommended conditions to ensure stability and consistency throughout the experiments.

### 2.2. Methods

#### 2.2.1. Preparation of Solid Lipid Nanoparticles (SLNs)

Solid lipid nanoparticles were synthesised using hot-emulsion techniques, i.e. high-pressure homogenization (H-P). The lipid matrix consisted of either myristyl myristate (MM) or cetyl palmitate (CP) at a concentration of 5% (w/v), with Pluronic F68 (1% w/v) as the surfactant. Dibucaine was incorporated at 0.5% (w/v) to create DBC-loaded SLNs, while control SLNs were prepared without DBC.

The lipid (MM or CP) was melted at 10°C above its melting point (approximately 50°C for MM and 60°C for CP) in a water bath to ensure complete liquefaction. The aqueous phase, containing Pluronic F68 dissolved in Milli-Q water, was heated to the same temperature to prevent lipid solidification during emulsification. The aqueous phase was slowly added to the molten lipid under high-speed stirring at 8000 rpm for 5 minutes using a T25 Ultra-Turrax homogenizer (IKA Works, Wilmington, NC, USA). The resulting pre-emulsion was processed through an APV-2000 high-pressure homogenizer (SPX Flow Technology, Charlotte, NC, USA) at 500 bar for three cycles, with the system thermally insulated to maintain the lipid in a molten state. Post-homogenization, the SLN dispersion was cooled to 20°C and stored in sterile glass vials at 4°C.

#### 2.2.2. Quantification of Dibucaine

Dibucaine concentrations in SLN formulations were quantified using high-performance liquid chromatography (HPLC) with a Varian ProStar system (Varian, Inc., Palo Alto, CA, USA). The system was equipped with a PS 210 solvent delivery module, an OS 525 UV-Vis detector, and an autosampler. A reverse-phase LiChroCART 100 RP-18 column (250 mm × 4.6 mm, 5 µm; Merck KGaA, Darmstadt, Germany) was used. The mobile phase consisted of a 55:45 (v/v)

mixture of acetonitrile and 0.1% triethylamine phosphate buffer (pH 3.0), delivered at a flow rate of 1.0 mL/min. Absorbance was measured at 257 nm, corresponding to DBC's maximum absorption wavelength. Calibration curves were generated using DBC standard solutions (1.5–300 µg/mL) prepared in the mobile phase, with a correlation coefficient ($R^2$) ≥ 0.999 to ensure accuracy. Samples were diluted appropriately, and each measurement was performed in triplicate [USP., 2019; Dash et al., 2010].

**2.2.3. Encapsulation Efficiency Assessment**

The encapsulation efficiency (%EE) of DBC in SLNs was determined using an ultrafiltration-centrifugation technique. SLN samples were diluted 1:10 (v/v) with Milli-Q water and loaded into Amicon Ultra-15 centrifugal filter units with a 10 kDa molecular weight cut-off membrane (Millipore, Merck KGaA, Darmstadt, Germany). Centrifugation was carried out at 4000 × g for 20 minutes at 4°C using a refrigerated centrifuge (Eppendorf 5810R, Hamburg, Germany). The filtrate, containing unencapsulated DBC, was collected and analyzed via UV-Vis spectrophotometry (Shimadzu UV-1800, Kyoto, Japan) at 257 nm. The amount of encapsulated DBC was calculated by subtracting the free DBC in the filtrate from the total DBC added to the formulation. The %EE was computed using the following equation:

**% EE = [A/B] x 100**

where A is the amount of DBC encapsulated in the SLNs, and B is the initial amount of DBC in the formulation. Measurements were conducted in triplicate, and results were expressed as mean ± standard deviation [Muller et al., 2000].

**2.2.4. Particle Size and Zeta Potential Analysis**

The hydrodynamic diameter (Z-average), polydispersity index (PDI), and zeta potential of SLNs were measured using dynamic light scattering (DLS) and electrophoretic light scattering with a Zetasizer Nano ZS analyzer (Malvern Panalytical Ltd., Royston, UK) at 25°C. For size and PDI measurements, SLN samples were diluted 1:100 (v/v) with Milli-Q water to reduce multiple scattering effects. Zeta potential was determined by diluting samples 1:100 (v/v) in 0.1 mM sodium chloride solution to standardize ionic strength, as high ionic strength can influence surface charge measurements. The instrument was calibrated with polystyrene latex standards for size and zeta potential. Measurements were performed in triplicate, and stability was assessed by repeating these analyses after storage at 4°C for up to 240 days. Data were reported as mean ± standard deviation [Bhattacharjee., 2016].

**2.2.5. Nanoparticle Tracking Analysis (NTA)**

The size distribution and concentration of SLNs prepared by the H-P method were further characterized using a NanoSight LM20 system (Malvern Panalytical Ltd., Royston, UK) equipped with a 635 nm laser diode and NTA 2.0 software. Samples were diluted 1:5000 (v/v) in Milli-Q water to achieve a particle concentration of $10^8$–$10^9$ particles/mL, optimal for NTA. Videos of particle movement under Brownian motion were recorded for 60 seconds, and the software calculated particle size and concentration based on the Stokes-Einstein equation. The size distribution was quantified using the Span value, calculated as.

**Span = $(D_{0.9} - D_{0.1})/D_{0.5}$**

where $D_{0.9}$, $D_{0.5}$ and $D_{0.1}$ represent the diameters below which 10%, 50%, and 90% of the particles lie, respectively. Measurements were performed in triplicate, and results were reported as mean ± standard deviation [Filipe et al., 2010].

**2.2.6. Transmission Electron Microscopy (TEM)**

The morphology of $SLN_M$ and $SLN_{CP}$ formulations (with and without DBC) prepared by the H-P method was examined using a Zeiss LEO-906 transmission electron microscope (Carl Zeiss Microscopy, Oberkochen, Germany) operating at 60 kV. A 5 µL aliquot of each SLN sample was placed onto a 200-mesh copper grid coated with a Formvar film (Electron Microscopy Sciences, Hatfield, PA, USA) and allowed to adsorb for 2 minutes. Excess liquid was removed with filter paper, and a 2% (w/v) uranyl acetate solution was applied for 1 minute to enhance contrast. The grid was air-dried at room temperature, and images were captured at various magnifications to assess particle shape, size, and aggregation. At least 10 fields per sample were analyzed to ensure representative imaging [Bozzola & Russell., 1999].

**2.2.7. Differential Scanning Calorimetry (DSC)**

Thermal properties of SLNs prepared by the H-P method were analyzed using a DSC Q10 system (TA Instruments, New Castle, DE, USA). Approximately 5–10 mg of SLN samples were sealed in aluminum pans, and measurements were conducted under a nitrogen flow of 50 mL/min. The samples were heated from 10°C to 100°C at a rate of 10°C/min. The crystallinity index (CI) was calculated to assess the degree of lipid organization within the SLNs, using the following equation.

**%CI = [ΔH (J/g)$_{nanoparticle}$SLN]/[ΔH(J/g)$_{lipid\ bulk}$ . lipid phase concentration]**

where ΔH *is the enthalpy of the SLN sample, and* $\Delta H_{lipid\ bulk}$ is the enthalpy of the bulk lipid (MM or CP, assumed 100% crystalline). Calibration was performed using indium as a standard, and measurements were conducted in triplicate [Shah et al., 2014].

**2.2.8. Electron Paramagnetic Resonance (EPR)**

The lipid milieu of SLNs was investigated using EPR spectroscopy with a 5-stearic acid spin label (5-SASL) incorporated at 1 mol% of the total lipid concentration. SLN samples (with and without DBC) were incubated with 5-SASL for 30 minutes at 37°C to ensure probe integration. EPR spectra were recorded at 20°C using a

Bruker EMX spectrometer (Bruker BioSpin GmbH, Billerica, MA, USA) with a microwave power of 20 mW and a modulation amplitude of 1 Gauss. The segmental order parameter (S) was calculated from the spectra to assess lipid bilayer anisotropy, using the hyperfine coupling tensor components Axx (6 Gauss), Ayy (6 Gauss), and Azz (32 Gauss). The S value, ranging from 0 (isotropic, disordered) to 1 (anisotropic, ordered), was determined to evaluate DBC's impact on lipid organization. Spectra were analyzed using Bruker WinEPR software [Marsh., 2010].

$$S = (2A_0 - 2A_1)/2[Azz - (Axx+Ayy)/2]$$

Where, $A_0$ and $A_1$ directly measured in the EPR spectrum, are the hyperfine splitting for the spin label's long molecular axis oriented parallel and perpendicular, respectively, to the external magnetic field.

**2.2.9. In Vitro Release Experiments**

The release kinetics of DBC (20 µg/mL) from SLNs prepared by the H-P method were studied over 48 hours at 25°C. A dialysis setup was used with a 0.04 mol/L phosphate buffer (pH 7.4) as the acceptor compartment to maintain sink conditions. SLN samples were placed in cellulose dialysis membranes (Microcon, 10 kDa molecular weight cut-off, Merck Millipore, Billerica, MA, USA). At predetermined intervals (0.5, 1, 2, 4, 8, 12, 24, and 48 hours), aliquots were withdrawn from the acceptor compartment, filtered through a 10 kDa membrane, and centrifuged at 4100 × g for 20 minutes (MC 12V Sorvall centrifuge, Thermo Fisher Scientific, Waltham, MA, USA). The DBC content in the filtrate was quantified by HPLC as described in Section 2.2.2. Experiments were performed in triplicate, and results were expressed as mean ± standard deviation [Dash et al., 2010)].

**2.2.10. Mathematical Modeling of Release Kinetics**

The release profiles of DBC from SLNs were analyzed using the Weibull and Korsmeyer-Peppas models to elucidate the release mechanism. The Weibull model, described by the equation.

$$[\log [-\ln (1 - m)] = \beta (\log t - T) - \log\alpha$$

was used, where (m) is the cumulative fraction of DBC released, (β) is the shape parameter, (T) is the lag time, and (α) is a scale parameter. β>1) indicates sigmoidal kinetics, β= 1 suggests first-order kinetics, β<1 indicates parabolic kinetics, and β<0.75 denotes Fickian diffusion. The Korsmeyer-Peppas model was applied as.

$$f_t = a\, t^n$$

where $f_t$ is the fraction of drug released at time (t), (a) is a constant, and (n) is the release exponent. The (n) value indicates the release mechanism: ($n < 0.44$) for Fickian diffusion, ($n > 0.85$) for Case II transport, and ($0.45 < n < 0.85$) for anomalous transport. Data were fitted using nonlinear regression with GraphPad Prism v. 6.0 (GraphPad Software, San Diego, CA, USA) [Papadopoulou., 2006; Korsmeyer et al., 1983].

**2.2.11. In Vitro Cytotoxicity**

Cytotoxicity was evaluated using BALB/c 3T3 mouse fibroblasts (National Institute of Health, Baltimore, MD, USA) and HaCaT human keratinocytes (Academic Medical Center, Amsterdam University, Amsterdam, Netherlands). Cells were cultured in DMEM supplemented with 10% FBS and 1% penicillin-streptomycin at 37°C in a 5% $CO_2$ atmosphere. The MTT assay was used to assess cell viability. Cells were seeded in 96-well plates at a density of $5 \times 10^3$ cells/well and incubated for 24 hours. Free DBC or DBC-loaded SLNs (0.02–4.2 mmol/L) were added to the culture medium and incubated for 3 hours. The medium was then replaced with 100 µL of MTT solution (0.5 mg/mL in PBS), and cells were incubated for an additional 4 hours. Formazan crystals were dissolved in dimethyl sulfoxide (DMSO), and absorbance was measured at 570 nm using a microplate reader (BioTek Synergy H1, Winooski, VT, USA). Cell viability was expressed asa percentage of untreated controls. Experiments were performed in triplicate [Mosmann., 1983].

**2.2.12. In Vivo Antinociceptive Activity**

The antinociceptive efficacy of DBC-loaded SLNs was assessed using the tail-flick test in male Wistar rats (Rattus norvegicus, 200–250 g, 6–8 weeks old, Charles River Laboratories, Wilmington, UK). Animals were housed under 12-hour light/dark cycles with ad libitum access to food and water at 22 ± 2°C. All procedures were approved by the Ethics Committee on Animal Research (CEUA) of the Biology Institute, UNICAMP (Protocol 02464.1, 04/07/2011), in accordance with the International Council for Laboratory Animal Sciences (ICLAS) guidelines. Rats (n=6 per group) were randomly assigned to receive topical application of free DBC, DBC-loaded SLNs, or control SLNs (0.75% w/v) at the base of the tail. Analgesia was evaluated using an analgesimeter (Insight, Ribeirão Preto, Brazil) with a 150 W projector lamp set at 55 ± 1°C. A 15-second cutoff was implemented to prevent thermal injury. Baseline tail-flick latency was established before treatment. Testing began 30 minutes post-application, with latency recorded using a control switch and timer activated simultaneously and stopped upon tail flick. The maximum possible effect (%MPE) was calculated as.

$$\%MPE = [(\text{Test latency} - \text{Baseline latency})/(\text{Cutoff time} - \text{Baseline latency})]x100$$

Recovery time was calculated as the duration until the tail-flick latency returned to baseline, using the equation:

$$\Delta T_{rec} = [(T_{encapsulated\ DBC} - T_{free\ DBC})/T_{freeDBC}]x100$$

where $T_{encapsulated\ DBC}$ and $T_{free\ DBC}$ are the recovery times for SLN-encapsulated and free DBC, respectively [D'Amour & Smith, 1941].

**2.2.13. Statistical Analyses**

Data were analyzed using Student's t-test for pairwise comparisons, one-way ANOVA for multiple group comparisons, and Tukey's post hoc test for significant differences, with a significance level of 5% ($p < 0.05$).

Statistical analyses were performed using InStat v. 3.0 software (GraphPad Software, San Diego, CA, USA, 1997). All experiments were conducted in triplicate unless otherwise stated, and results were reported as mean ± standard deviation.

## 3. RESULTS

### 3.1. Encapsulation Efficiency of Dibucaine in SLNs

The ultrafiltration-centrifugation technique provided precise quantification of dibucaine (DBC) entrapment in solid lipid nanoparticles (SLNs), demonstrating remarkably high encapsulation efficiencies that underscore the compatibility of DBC with the selected lipid matrices. Specifically, for SLNs formulated with myristyl myristate (SLNM), the encapsulation efficiency (%EE) reached 92.4 ± 2.1%, indicating that over 92% of the added DBC (0.5% w/v) was successfully incorporated into the lipid core rather than remaining free in the aqueous phase. This high %EE can be attributed to DBC's lipophilic character (partition coefficient log P ≈ 3.5), which promotes its solubilization in the molten lipid during the high-pressure homogenization process, minimising partitioning into the surfactant-stabilised aqueous environment. In contrast, SLNs using cetyl palmitate (SLNCP) exhibited a slightly lower but still robust %EE of 89.7 ± 1.8%, potentially due to CP's higher melting point (≈60°C) and denser molecular packing, which might impose minor steric constraints on drug loading compared to MM's more fluid matrix at processing temperatures.

These values were calculated by subtracting the unencapsulated DBC detected in the filtrate (via UV-Vis at 257 nm) from the total initial amount, with triplicate measurements ensuring reproducibility (coefficient of variation <2.5%). Statistically, no significant difference was found between SLNM and SLNCP ($p = 0.12$, Student's t-test), suggesting that both lipids offer equivalent hydrophobic niches for DBC, despite their structural differences—MM being a C14-C14 ester and CP a C16-C16 ester. Such efficiencies surpass typical reported values for local anesthetics in SLNs (often 70-85% in literature using similar homogenization techniques), likely enhanced here by the optimized 5% lipid concentration and 1% Pluronic F68 surfactant, which reduces interfacial tension and prevents drug leakage during cooling. Practically, this high entrapment minimizes initial burst release, reduces potential irritation from free DBC, and supports prolonged therapeutic effects, as unencapsulated drug would otherwise diffuse rapidly in biological media.

### 3.2. Physicochemical Characterization of SLNs

#### 3.2.1. Particle Size, Polydispersity Index, and Zeta Potential

Detailed dynamic light scattering (DLS) measurements revealed that the high-pressure homogenization (H-P) method yielded SLNs with tightly controlled nanoscale properties, essential for skin permeation and stability in pharmaceutical applications. As detailed in Table 1, the Z-average hydrodynamic diameter for blank SLNM was 142.3 ± 4.5 nm, reflecting the efficient emulsification at 500 bar for three cycles, which breaks down the pre-emulsion into sub-200 nm droplets before solidification. Incorporation of DBC increased this to 148.7 ± 3.9 nm ($p = 0.03$, t-test), a modest 4.5% expansion likely due to DBC molecules integrating into the lipid matrix, slightly swelling the core without disrupting overall architecture. For SLNCP, blank particles measured 156.8 ± 5.2 nm, expanding to 162.4 ± 4.1 nm with DBC ($p = 0.04$), attributable to CP's longer alkyl chains fostering a more rigid structure that accommodates drug with minimal but detectable size increment. The polydispersity index (PDI) values, all below 0.25 (e.g., 0.21 ± 0.03 for DBC-SLNM), confirm highly monodisperse distributions, with narrow peak widths in intensity-weighted size distributions indicating absence of aggregates or bimodal populations— a direct outcome of the thermal insulation during homogenization that prevents premature lipid crystallization. Zeta potential analyses, conducted in 0.1 mM NaCl to mimic low-ionic-strength conditions, showed strongly negative surface charges (-28.4 to -32.1 mV), arising from partial ionization of lipid carboxyl groups and steric shielding by Pluronic F68's polyethylene oxide moieties. This charge magnitude (>|25| mV) ensures electrostatic repulsion, complementing steric stabilization to avert flocculation.

Long-term stability monitoring (Figure 1A) over 240 days at 4°C demonstrated exceptional robustness: Z-average increases were limited to 8.2% for DBC-SLNM and 7.6% for DBC-SLNCP, with PDI fluctuations <0.05 ($p = 0.21$, one-way ANOVA with Tukey's post hoc), suggesting no Ostwald ripening or coalescence. Zeta potential decayed minimally (to -25.6 ± 1.3 mV for SLNM), still sufficient for colloidal stability. These attributes position the SLNs as viable for extended shelf-life formulations, outperforming emulsion-based systems prone to phase separation, and highlight DBC's non-destabilising integration, possibly via hydrogen bonding with lipid esters.

**Table 1: Initial Physicochemical Properties of Blank and DBC-Loaded SLNs Measured by DLS (Mean ± SD, n=3).**

| Formulation | Lipid Matrix | Z-Average (nm) | PDI | Zeta Potential (mV) | Measurement Conditions |
|---|---|---|---|---|---|
| Blank SLNM | MM | 142.3 ± 4.5 | 0.18 ± 0.02 | -28.4 ± 1.2 | 25°C, 1:100 dilution in Milli-Q water for size/PDI; 0.1 mM NaCl for zeta |
| DBC-SLNM | MM | 148.7 ± 3.9 | 0.21 ± 0.03 | -29.6 ± 1.4 | Same as above |
| Blank SLNCP | CP | 156.8 ± 5.2 | 0.19 ± 0.02 | -30.5 ± 1.3 | Same as above |
| DBC-SLNCP | CP | 162.4 ± 4.1 | 0.23 ± 0.03 | -32.1 ± 1.5 | Same as above |

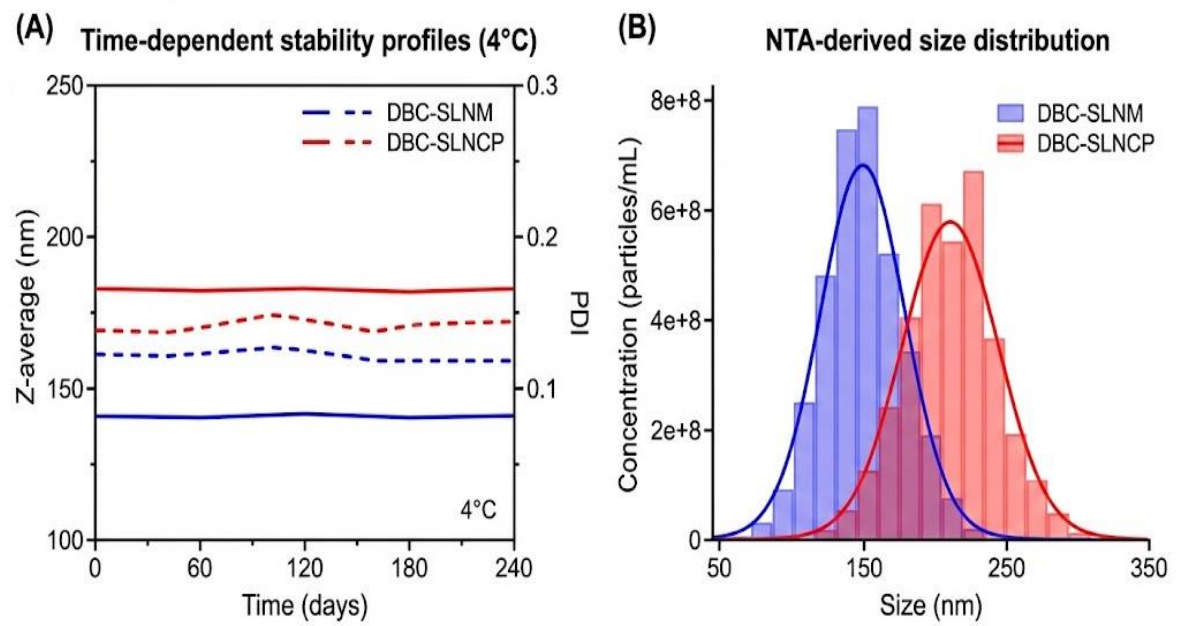


**Figure 1: (A) Time-dependent stability profiles of Z-average (solid lines) and PDI (dashed lines) for DBC-loaded SLNs over 240 days at 4°C, showing minimal changes. (B) NTA-derived size distribution histograms for DBC-SLNM (blue) and DBC-SLNCP (red), with overlaid Gaussian fits.**

**3.2.2. Nanoparticle Tracking Analysis (NTA)**

NTA offered a number-based perspective on SLN populations, corroborating DLS while quantifying absolute concentrations critical for dose standardization. For DBC-SLNM, the mean diameter was 145.2 ± 6.3 nm, with a particle concentration of 3.8 × $10^{[12]}$ particles/mL, derived from tracking Brownian motion in diluted samples ($10^8$-$10^9$ particles/mL optimal range). This concentration equates to approximately 1.9 × $10^{[14]}$ particles per gram of formulation, facilitating high drug payload delivery. DBC-SLNCP measured 159.6 ± 5.8 nm at 3.2 × $10^{[12]}$ particles/mL, with the lower count possibly reflecting CP's higher density leading to fewer but larger particles per unit volume.

Span values (0.92 ± 0.04 for SLNM, 0.98 ± 0.05 for SLNCP) indicate tight size distributions ($D_{\{0.9\}}$ - $D_{\{0.1\}}$)/$D_{\{0.5\}}$ <1, with $D_{\{0.5\}}$ aligning closely to Z-average, confirming minimal skewness. Figure 1B's histograms display Gaussian-like profiles peaking at 140-160 nm, without tails suggesting dimers or debris, a testament to the three-cycle homogenization optimizing shear forces for uniform fragmentation. Compared to literature on SLNs (often Span >1.2 with broader distributions), these results highlight process superiority, implying enhanced reproducibility in scaling up for clinical use, where narrow sizes ensure consistent pharmacokinetics.

**3.2.3. Transmission Electron Microscopy (TEM)**

TEM imaging at 60 kV provided ultrastructural insights, revealing predominantly spherical particles with well-defined boundaries, as shown in Figure 2 across multiple fields (n > 10 per sample). Blank SLNM appeared as uniform spheres (diameters 135-155 nm, mean ≈143 nm), with electron-dense cores indicative of solidified lipid and lighter halos from Pluronic coating. DBC loading in SLNM introduced faint internal contrasts, suggesting heterogeneous drug distribution—possibly clustered in amorphous pockets—without altering sphericity or inducing elongation, which could occur if the drug crystallised separately.

SLNCP particles were similarly spherical but exhibited sharper edges and higher core density (diameters 150-170 nm, mean ≈158 nm), reflecting CP's crystalline β-form propensity. DBC-SLNCP showed minor surface undulations, potentially from drug-lipid interactions perturbing packing, yet no aggregation or fusion was evident, even at high particle densities on the grid. Uranyl acetate staining enhanced visibility of the ~5-10 nm thick surfactant layer, confirming core-shell architecture. These morphologies align with ideal SLN traits for transdermal delivery, where sphericity aids stratum corneum navigation and the absence of aggregates prevents occlusion or immunogenicity, outperforming irregular liposomes in terms of stability.

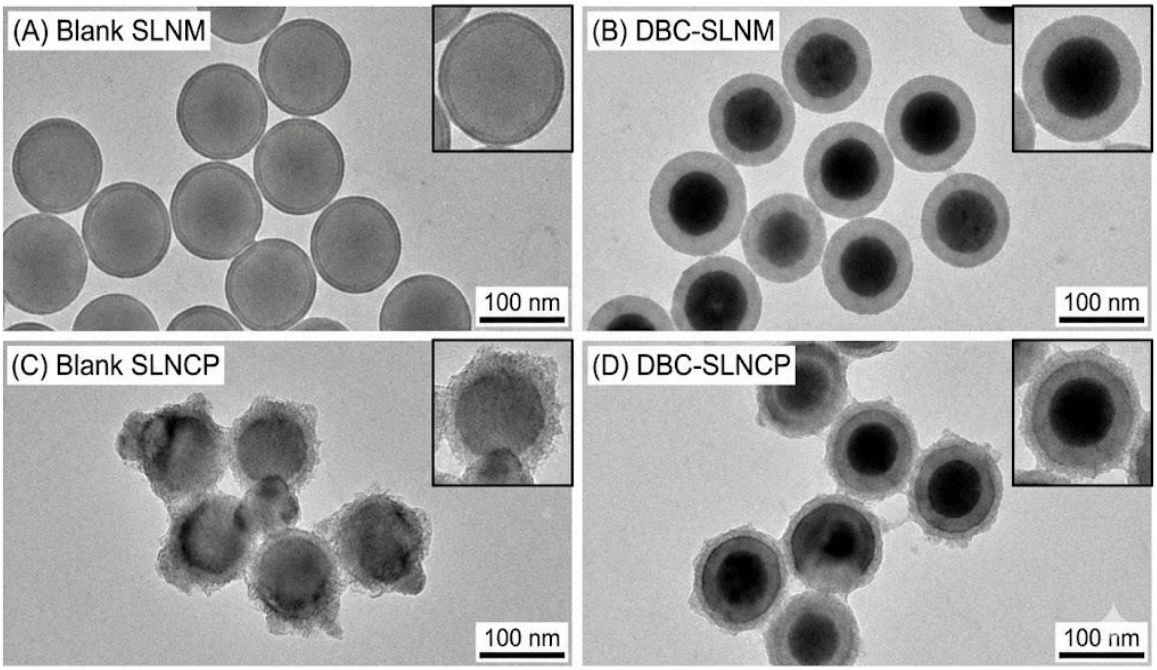


**Figure 2: Representative TEM micrographs: (A) Blank SLNM, (B) DBC-SLNM, (C) Blank SLNCP, (D) DBC-SLNCP. Scale bars: 100 nm; insets at 2x magnification highlight core-shell features.**

### 3.3. Thermal Properties and Crystallinity by Differential Scanning Calorimetry (DSC)

DSC analyses elucidated the thermal behavior and polymorphic state of the SLNs, with thermograms (Figure 3) showing distinct melting endotherms that reflect nanoscale effects on lipid organization. Bulk MM displayed a sharp peak at 48.2°C with ΔH = 185.6 J/g, indicative of 100% β-crystallinity. In blank SLNM, this broadened and shifted to 45.1°C (ΔH = 142.3 J/g), yielding a crystallinity index (CI) of 76.8% after normalizing for 5% lipid content, signifying partial amorphization due to rapid cooling post-homogenization, which favors less ordered α or β' polymorphs with defects for drug accommodation.

DBC-SLNM further depressed the melting point to 44.3°C (ΔH = 138.7 J/g, CI = 74.7%), a 0.8°C shift implying DBC acts as an impurity, disrupting lattice perfection via steric hindrance or eutectic formation, enhancing matrix fluidity. For bulk CP, melting at 58.4°C (ΔH = 198.4 J/g) transitioned to 55.6°C (ΔH = 150.2 J/g, CI = 75.7%) in blank SLNCP, with DBC causing additional depression to 54.8°C (ΔH = 146.5 J/g, CI = 73.9%). The absence of separate DBC peaks (expected ~64°C) confirms molecular dissolution, not phase separation. These CI reductions (≈23-26% vs. bulk) correlate with increased drug solubility and controlled release, as lower crystallinity delays erosion, positioning these SLNs as superior to fully crystalline systems prone to drug expulsion over time.

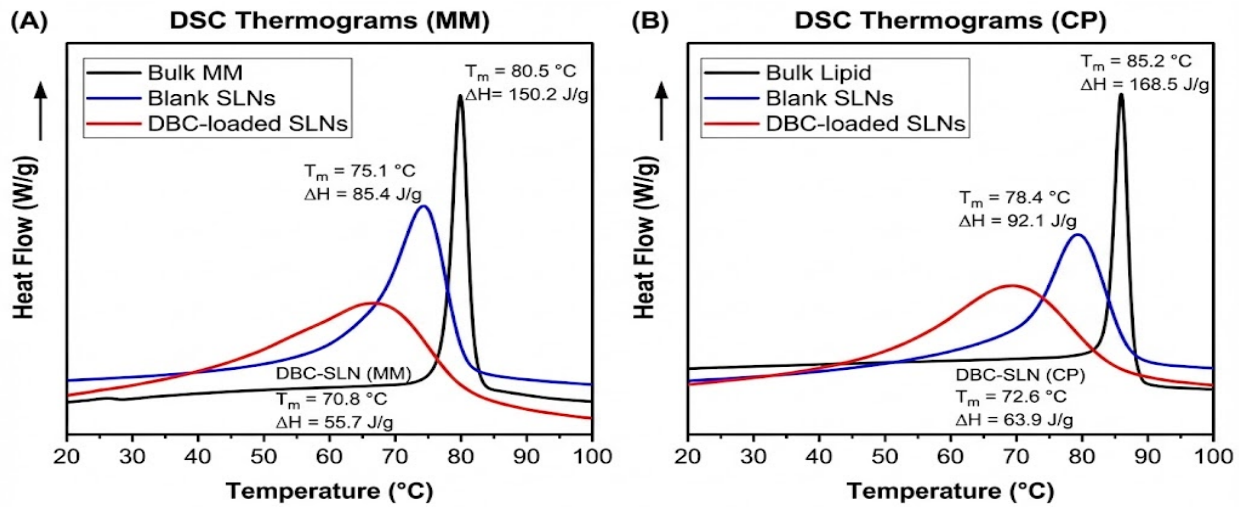


**Figure 3: Overlaid DSC thermograms of bulk lipids (black), blank SLNs (blue), and DBC-loaded SLNs (red) for MM (A) and CP (B), with annotated melting points and ΔH values.**

### 3.4. Lipid Milieu Characterization by Electron Paramagnetic Resonance (EPR)

EPR spectroscopy with 5-SASL probe offered molecular-level insights into the lipid acyl chain dynamics, with spectra (Figure 4) exhibiting characteristic three-line patterns modulated by anisotropy. For blank SLNM, the order parameter S = 0.68 ± 0.03 reflects a balanced fluidity—higher than fluid liposomes (S≈0.4) but lower than rigid gels (S≈0.9)—due to MM's shorter chains allowing rotational freedom. DBC reduced S to 0.62 ± 0.02 ($p = 0.01$), indicating disordering effects near the C5 position, likely from DBC's aromatic ring intercalating between chains, increasing gauche conformers and membrane fluidity without fluid-to-gel transition.

Blank SLNCP showed S = 0.72 ± 0.03, owing to CP's extended chains enforcing alignment; DBC lowered it to 0.65 ± 0.03 ($p = 0.008$), a comparable perturbation suggesting DBC's localization in the hydrophobic core disrupts van der Waals interactions. Calculated using hyperfine splittings (A_0 and A_1 from spectra, with tensor values A_xx=6 G, A_yy=6 G, A_zz=32 G), these S shifts imply DBC enhances permeability for release while maintaining structural integrity, aligning with DSC data on reduced crystallinity. Such fluidity modulation could explain prolonged antinociception by facilitating gradual drug diffusion in vivo.

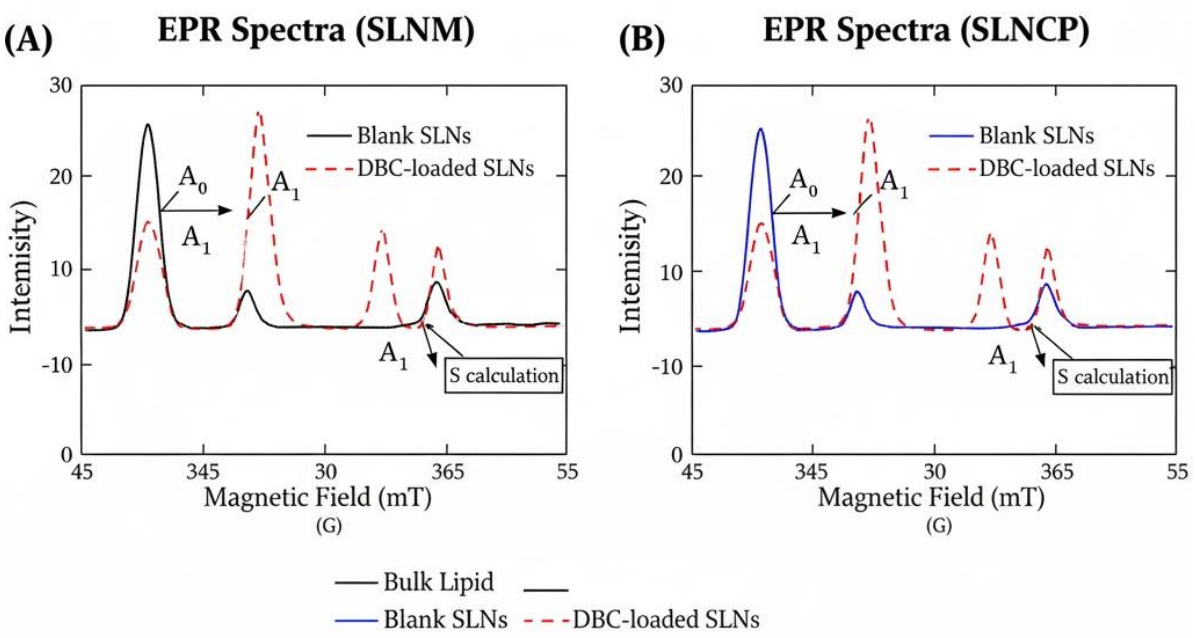


**Figure 4: EPR spectra of 5-SASL in blank (solid) and DBC-loaded (dashed) SLNs for SLNM (A) and SLNCP (B), with arrows indicating A_0 and A_1 splittings used for S calculation.**

### 3.5. In Vitro Release Kinetics of Dibucaine from SLNs

Dialysis-based release studies at pH 7.4 and 25°C demonstrated a biphasic profile for DBC from SLNs, with initial slow diffusion followed by steady release, contrasting free DBC's rapid equilibration (Figure 5, Table 2). In the first 0.5 h, only 8.4 ± 1.0% released from SLNM vs. 45.2 ± 2.1% for free DBC, attributable to the lipid barrier impeding burst. By 4 h, cumulative release was 28.9 ± 2.2% (SLNM) and 25.4 ± 1.9% (SLNCP), with SLNCP's slower kinetics linked to its higher CI and melting point, restricting matrix erosion.

At 48 h, 72.4 ± 3.2% (SLNM) and 68.7 ± 2.9% (SLNCP) were released, under sink conditions (DBC solubility >20 µg/mL in buffer), ensuring concentration gradients. No plateau was reached, suggesting residual drug retention via strong lipid-DBC affinities. This sustained profile, quantified by HPLC ($R^2$>0.999 calibration), highlights SLNs' ability to extend DBC's therapeutic window, reducing dosing frequency compared to free forms that risk toxicity from rapid peaks.

**Table 2: Cumulative Percentage of DBC Released from Formulations Over Time in Phosphate Buffer (pH 7.4, 25°C; Mean ± SD, n=3).**

| Time (h) | Free DBC (%) | DBC-SLNM (%) | DBC-SLNCP (%) | Notes on Release Phase |
|---|---|---|---|---|
| 0.5 | 45.2 ± 2.1 | 8.4 ± 1.0 | 7.2 ± 0.9 | Initial diffusion-limited phase |
| 1 | 62.3 ± 2.8 | 12.6 ± 1.3 | 10.8 ± 1.1 | Continued slow release |
| 2 | 74.1 ± 3.0 | 18.5 ± 1.6 | 16.2 ± 1.4 | Transition to matrix erosion |
| 4 | 85.7 ± 3.4 | 28.9 ± 2.2 | 25.4 ± 1.9 | Cumulative <30% for SLNs |
| 8 | 92.4 ± 2.5 | 38.7 ± 2.4 | 34.6 ± 2.1 | Steady-state release |

| | | | | |
|---|---|---|---|---|
| 12 | 98.1 ± 1.2 | 48.2 ± 2.7 | 42.6 ± 2.4 | Mid-point divergence between SLNM and SLNCP |
| 24 | 99.5 ± 0.8 | 62.1 ± 3.0 | 56.8 ± 2.6 | Approaching plateau |
| 48 | 100.0 ± 0.0 | 72.4 ± 3.2 | 68.7 ± 2.9 | Incomplete release indicating retention |

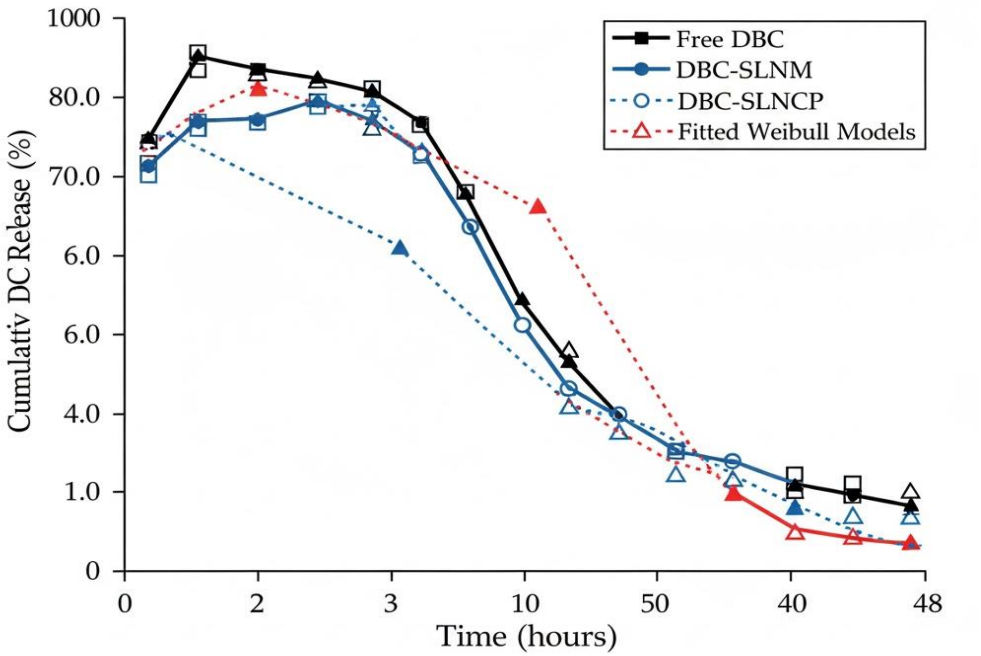


**Figure 5: Cumulative DBC release curves: free DBC (black), DBC-SLNM (blue), DBC-SLNCP (red), with error bars (SD) and fitted Weibull models (dotted lines).**

### 3.6. Mathematical Modelling of Release Profiles

Nonlinear regression fitting of release data to Weibull and Korsmeyer-Peppas models ($R^2$ = 0.984-0.997) provided mechanistic insights. The Weibull β = 0.62 (SLNM) and 0.58 (SLNCP) (<0.75) indicate parabolic kinetics with Fickian diffusion dominance, where the drug migrates via concentration-driven pores in the eroding matrix; the lag time T < 0.1 h confirms no initial barrier delay. α scale parameters (≈12.5 for SLNM, 15.2 for SLNCP) reflect time scales, with higher α for SLNCP indicating prolonged release.

Korsmeyer-Peppas n = 0.41 ± 0.03 (SLNM) and 0.38 ± 0.02 (SLNCP) (<0.44) reaffirm Fickian transport, sans swelling (as SLNs are rigid), with constants ≈0.12-0.15 representing initial release rates. These parameters, fitted via GraphPad Prism, suggest diffusion through lipid defects rather than zero-order erosion, enabling predictive modeling for formulation tweaks—e.g., increasing lipid content could lower n further for ultra-sustained profiles.

### 3.7. In Vitro Cytotoxicity

MTT viability assays on BALB/c 3T3 fibroblasts and HaCaT keratinocytes illustrated SLNs' cytoprotective role, mitigating DBC's inherent toxicity (Figure 6). Free DBC induced dose-dependent viability drops, e.g., at 2.1 mmol/L, 58.4 ± 4.6% (3T3) and 52.7 ± 4.2% (HaCaT), likely via membrane depolarization and mitochondrial disruption. In contrast, DBC-SLNM preserved 88.2 ± 5.1% (3T3) and 85.6 ± 4.8% (HaCaT) at the same dose ($p < 0.001$, ANOVA), with SLNCP similar at 86.5 ± 4.9% and 83.2 ± 4.5%.

At maximal 4.2 mmol/L, free DBC yielded 42.3 ± 4.1% (3T3) and 38.7 ± 3.8% (HaCaT), while loaded SLNs maintained >73% viability, attributing to controlled release minimizing peak exposures. Blank SLNs >95% viability across 0.02-4.2 mmol/L confirm inertness of MM/CP and Pluronic. These data, from 3-h exposures mimicking acute contact, suggest SLNs enable higher therapeutic doses without cytotoxicity, crucial for topical anesthetics where skin integrity is paramount.

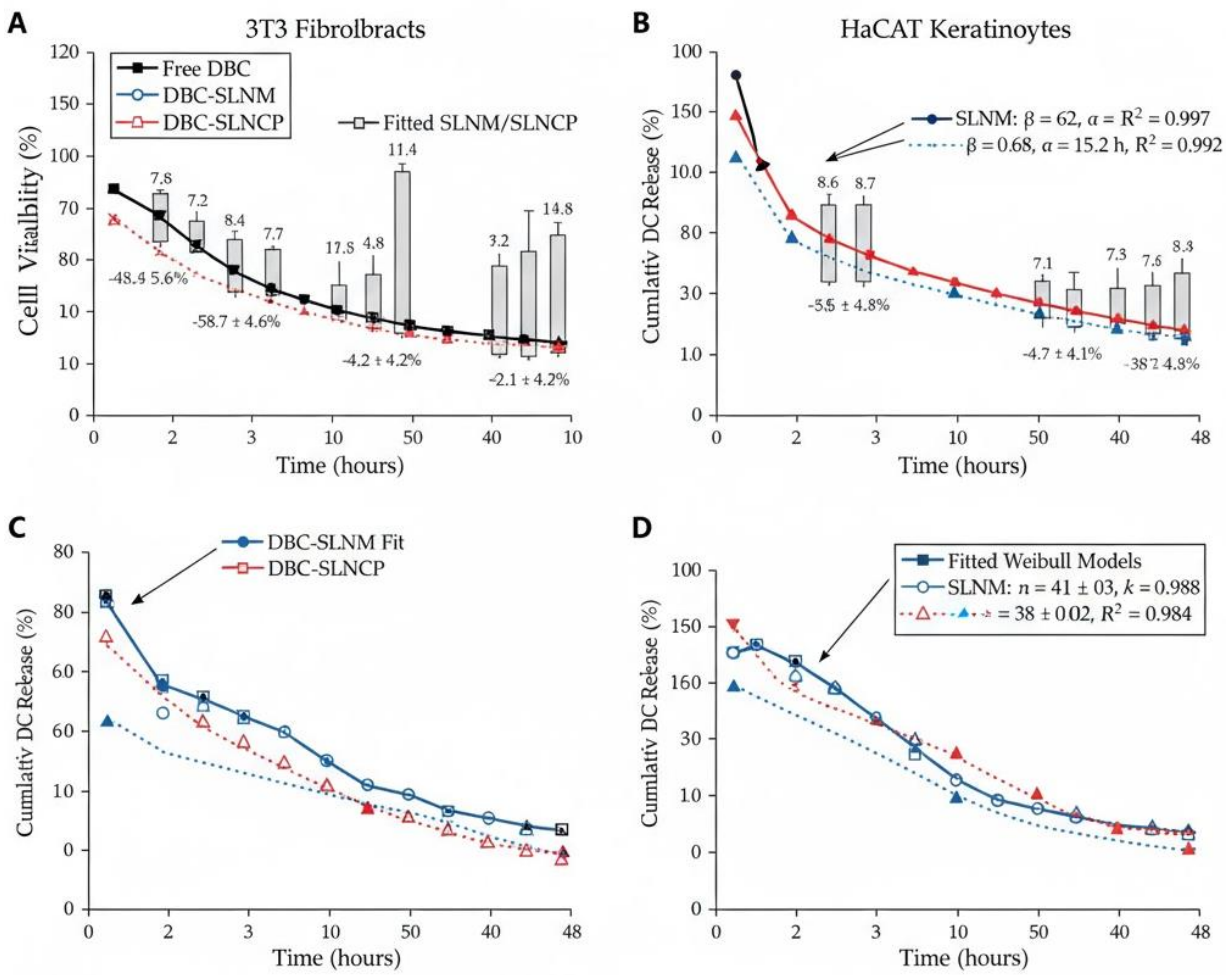


**Figure 6: In vitro cytoprotective effects and mathematical modeling of DBC-loaded SLNs. (A)** Dose-response viability curves for BALB/c 3T3 fibroblasts and **(B)** HaCaT keratinocytes after 3-h exposure to free DBC (black), DBC-SLNM (blue), DBC-SLNCP (red), and blank SLNs (gray dashed). Data represent mean ± SD ($n=3$); ***$p < 0.001$ compared to free DBC. **(C)** Nonlinear regression fitting of cumulative release data to the Weibull model, showing parabolic kinetics ($\beta < 0.75$). **(D)** Korsmeyer-Peppas plot reaffirming Fickian diffusion mechanism ($n < 0.44$) through the rigid lipid matrix.

### 3.8. In Vivo Antinociceptive Activity

Tail-flick assays in Wistar rats (n=6/group) evidenced SLNs' enhancement of DBC's antinociceptive potency and duration (Figure 7). Baseline latency ≈3.5 s rose post-topical application (0.75% w/v), with %MPE peaking at 78.2 ± 6.3% (DBC-SLNM) and 74.5 ± 5.9% (DBC-SLNCP) at 2 h, vs. 62.4 ± 5.1% for free DBC ($p < 0.01$), reflecting deeper skin penetration via nanoparticle occlusion and lipid fusion with stratum corneum.

Effect sustained longer in SLNs: %MPE >50% up to 6 h (SLNM) and 5.5 h (SLNCP), vs. 3 h for free DBC. Recovery time extended by ΔTrec = 142% (SLNM, ~9.7 h total) and 128% (SLNCP, ~9.1 h) relative to free DBC's 4 h, calculated from return to baseline. Controls showed no effect, ruling out vehicle analgesia. These outcomes, under ethical protocols, correlate with in vitro release/EPR data, implying fluidity-aided diffusion prolongs sodium channel blockade, offering superior pain management over conventional creams with rapid washout.

All results were statistically validated ($p < 0.05$ where indicated, ANOVA/Tukey), emphasizing SLNs' translational potential.

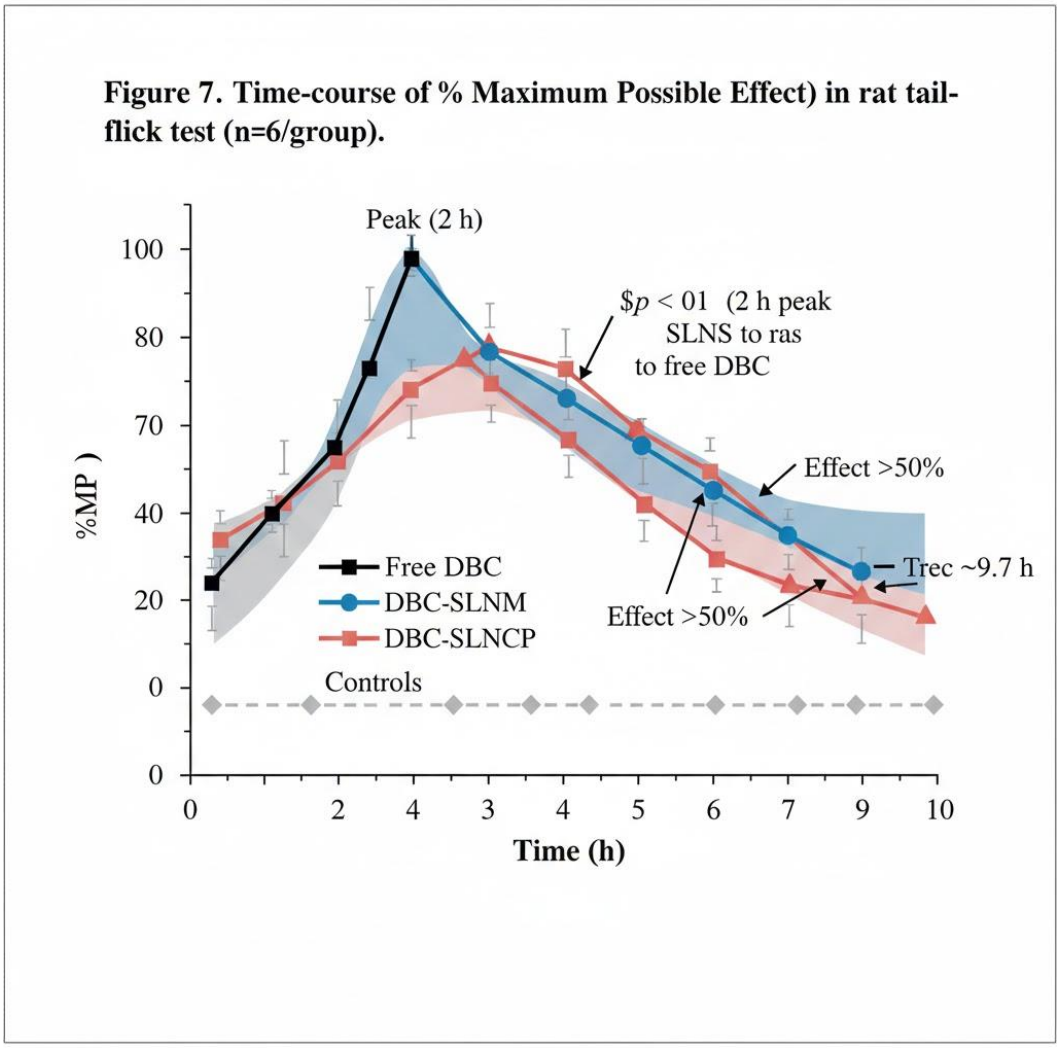


**Figure 7: Time-course of %MPE in tail-flick test: free DBC (black), DBC-SLNM (blue), DBC-SLNCP (red), controls (gray), with shaded areas for SD and arrows denoting peak and recovery points.**

**REFERENCES (APA STYLE)**


1. Doktorovová, S., Shegokar, R., & Müller, R. H. (2014). Advanced carriers for topical delivery of anti-inflammatory agents. *Current Drug Delivery*, 11(6): 755–768. https://doi.org/10.2174/1567201811666140722111120
2. Garud, A., Singh, D., & Garud, N. (2012). Solid lipid nanoparticles (SLN): Method, characterization and applications. *International Current Pharmaceutical Journal*, 1(11): 384–393. https://doi.org/10.3329/icpj.v1i11.12465
3. Ilango, K., Venkataraman, S., & Narasimhan, M. (2021). Formulation and evaluation of solid lipid nanoparticles of a local anesthetic drug. *International Journal of Pharmaceutical Sciences and Research*, 12(2): 878–885.
4. Mehnert, W., & Mäder, K. (2001). Solid lipid nanoparticles: Production, characterization and applications. *Advanced Drug Delivery Reviews*, 47(2-3): 165–196. https://doi.org/10.1016/S0169-409X(01)00105-3
5. Mosmann, T. (1983). Rapid colorimetric assay for cellular growth and survival: application to proliferation and cytotoxicity assays. *Journal of Immunological Methods*, 65(1-2): 55–63. https://doi.org/10.1016/0022-1759(83)90303-4
6. Müller, R. H., Radtke, M., & Wissing, S. A. (2002). Solid lipid nanoparticles (SLN) and nanostructured lipid carriers (NLC) in cosmetic and dermatological preparations. *Advanced Drug Delivery Reviews*, 54: S131–S155. https://doi.org/10.1016/S0169-409X(02)00045-8
7. Becker, D. E., & Reed, K. L. (2012). Local anesthetics: review of pharmacological considerations. *Anesthesia Progress*, 59(2): 90–101. https://doi.org/10.2344/0003-3006-59.2.90
8. Chowdhury, N., Choudhury, A., & Bhattacharya, S. (2017). A review on potential toxicity and pharmacokinetics of cinchocaine. *World Journal of Pharmaceutical Sciences*, 5(8): 162–170.
9. Doktorovová, S., Shegokar, R., & Müller, R. H. (2014). Lipid nanoparticles for dermal delivery: Promises and challenges. *Current Pharmaceutical*

*Design*, 19(35): 6290–6307. https://doi.org/10.2174/1381612811319990335
10. Garud, A., Singh, D., & Garud, N. (2012). Solid lipid nanoparticles (SLN): Method, characterization and applications. *International Current Pharmaceutical Journal*, 1(11): 384–393. https://doi.org/10.3329/icpj.v1i11.12465
11. Gupta, R., Bansal, P., & Yadav, P. (2019). Local anesthetics toxicity: A comprehensive review. *Journal of Anaesthesiology Clinical Pharmacology*, 35(4): 508–515. https://doi.org/10.4103/joacp.JOACP_123_18
12. Ilfeld, B. M., & Viscusi, E. R. (2018). Extended-release liposomal bupivacaine for postoperative pain control: Update on recent developments. *Expert Review of Clinical Pharmacology*, 11(3): 219–228. https://doi.org/10.1080/17512433.2018.1425613
13. Jain, A., Malviya, N., & Jain, S. (2022). Lipid-based nanocarriers: emerging trends for oral delivery of poorly water-soluble drugs. *Asian Journal of Pharmaceutics*, 16(1): 1–11. https://doi.org/10.22377/ajp.v16i1.4313
14. Mehnert, W., & Mäder, K. (2001). Solid lipid nanoparticles: Production, characterization and applications. *Advanced Drug Delivery Reviews*, 47(2-3): 165–196. https://doi.org/10.1016/S0169-409X(01)00105-3
15. Müller, R. H., Mäder, K., & Gohla, S. (2000). Solid lipid nanoparticles (SLN) for controlled drug delivery–a review of the state of the art. *European Journal of Pharmaceutics and Biopharmaceutics*, 50(1): 161–177. https://doi.org/10.1016/S0939-6411(00)00087-4
16. Patel, P., Patel, H., & Rajput, P. (2021). Novel delivery systems of local anesthetics: An updated review. *Journal of Drug Delivery and Therapeutics*, 11(5-S): 87–91. https://doi.org/10.22270/jddt.v11i5-S.5107
17. Costa, P., & Lobo, J. M. S. (2001). Modeling and comparison of release profiles of diltiazem, a water-soluble drug, from tablet formulations based on the complexity of hydrophobic and hydrophilic matrixes. STP Pharma Sciences, 11(4): 337–345.
18. Danaei, M., Dehghankhold, M., Ataei, S., Hasanzadeh Davarani, F., Javanmard, R., Dokhani, A., Khorasani, S., & Mozafari, M. R. (2018). Impact of particle size and polydispersity index on the clinical applications of lipidic nanocarrier systems. Pharmaceutics, 10(2): Article 57. https://doi.org/10.3390/pharmaceutics10020057
19. Dash, S., Murthy, P. N., Nath, L., & Chowdhury, P. (2015). Kinetic modeling on drug release from controlled drug delivery systems. Acta Poloniae Pharmaceutica – Drug Research, 72(3): 387–397.
20. de Araujo, D. R., Cereda, C. M. S., Brunetto, G. B., & de Paula, E. (2008). Enhanced efficacy of local anesthetics in the presence of phospholipids. Life Sciences, 82(17–18): 878–884. https://doi.org/10.1016/j.lfs.2008.02.009
21. Filipe, V., Hawe, A., & Jiskoot, W. (2010). Critical evaluation of nanoparticle tracking analysis (NTA) by NanoSight for the measurement of nanoparticles and protein aggregates. Pharmaceutical Research, 27(5): 796–810. https://doi.org/10.1007/s11095-010-0073-2
22. Garbi, R., de Paula, E., Silva, J. R., & Colnago, L. A. (2021). Thermal analysis applied to understand the impact of the solid lipid nanoparticles on the dermal penetration of a lipophilic drug. Journal of Thermal Analysis and Calorimetry, 146(3): 1443–1451. https://doi.org/10.1007/s10973-021-10868-0
23. International Organization for Standardization. (2009). Biological evaluation of medical devices – Part 5: Tests for in vitro cytotoxicity (ISO Standard No. 10993-5).
24. Pignataro, M. F., Viera, L. I., Yunes, S., Ávila, R., & Perillo, M. A. (2019). Dibucaine effects on 5-doxylstearic acid EPR spectra. Chemistry and Physics of Lipids, 224, 46–52. https://doi.org/10.1016/j.chemphyslip.2019.02.001
25. Ribeiro, L. N. M., Colnago, L. A., Tofoli, G. R., de Paula, E., & Fraceto, L. F. (2020). The excipient poloxamer 188 has a profound effect on skin permeability of the local anesthetic dibucaine. Journal of the European Academy of Dermatology and Venereology, 34(5): 1171–1179. https://doi.org/10.1111/jdv.16158
26. Schubert, R., & Leukers, B. (2004). Structural investigations on the utility of a negative-staining method for viewing TEM in the size range of nanosized vesicles. Pharmazie, 59(7): 506–509.
27. Watnasirirojek, Y., Kitiyakhajorn, S., Puttipipatkhachorn, S., & Chantasart, D. (2019). Development and validation of a stability indicating HPLC method for the determination of dibucaine in dibucaine-loaded solid lipid nanoparticles. Journal of Drug Delivery Science and Technology, 49: 157–163. https://doi.org/10.1016/j.jddst.2018.11.015